



Mechanical behaviour of wood T-joints. Experimental and numerical investigation

C.L. dos Santos, J.J.L. Morais

Engineering Department, School of Science and Technology, University of Trás-os-Montes e Alto Douro, Quinta de Prados, 5000-801 Vila Real, Portugal

University of Trás-os-Montes e Alto Douro, CITAB, Quinta de Prados, 5000-801 Vila Real, Portugal
clsantos@utad.pt

A.M.P. de Jesus

Engineering Department, School of Science and Technology, University of Trás-os-Montes e Alto Douro, Quinta de Prados, 5000-801 Vila Real, Portugal

IDMEC, Pólo-FEUP, Rua Dr. Roberto Frias, 4200-465 Porto, Portugal

ABSTRACT. Results of a double-shear single-dowel wood connection tested under monotonic quasi-static compression loading are presented and discussed in this paper. The wood used in this study was a pine wood, namely the *Pinus pinaster* species, which is one of the most important Portuguese species. Each connection (specimen) consists of three wood members: a centre member, loaded in compression along the parallel-to-grain direction and two simply supported side members, loaded along the perpendicular-to-grain direction (T-connection). The load transfer between wood members was assured by means of a steel dowel, which is representative of the most common joining technique applied for structural details in wooden structures. The complete load-slip behaviour of the joint is obtained until failure. In particular, the values of the stiffness, the ultimate loads and the ductility were evaluated. Additionally, this investigation proposed non-linear 3D finite element models to simulate the T-joint behaviour. The interaction between the dowel and the wood members was simulated using contact finite elements. A plasticity model, based on Hill's criterion, was used to simulate the joint ductility and cohesive damage modelling was applied to simulate the brittle failure modes (splitting) observed in the side members of the joint. The simulation procedure allowed a satisfactory description of the non-linear behaviour of the T-joint including the collapse prediction.

KEYWORDS. Maritime pine wood (*Pinus pinaster* Ait.); Dowel-type connections; T-connections; Finite Element Analysis; Hill Plasticity model; Cohesive damage models.

INTRODUCTION

The connections are frequently the critical elements of timber structures, being responsible for the reduction of continuity and global structural strength, requiring oversized structural elements. About 80% of failures observed in timber structures are due to connections [1]. Dowel-type timber connections are the most common

connections applied in timber structures. The singularity of this type of timber connections is associated to the combination of very distinct materials – wood and steel – and to the high anisotropy of wood. The knowledge of the mechanical behaviour of these dowel-type connections (e.g. load–slip relation, stress distribution, ultimate strength and failure modes) is of primordial importance for their rational application. This complex behaviour is governed by several geometric, material and load parameters (e.g. wood species, dowel diameter, end and edge distances, space between connectors, number of connectors, hole/dowel clearance, friction and load configuration).

According to design codes of current practice [2, 3], the design of dowel-type timber connections has been based on the European Yield Model (EYM) proposed by Johansen [4]. According to the EYM, the embedding strength of wood is a material parameter governing the failure of wood members. This model has an empirical basis and assumes an elastic-perfectly plastic behaviour for both wood and dowel. It also considers that embedding strength is a material property, when in fact it is a combination of several geometric and material parameters. The EYM only predicts the ultimate loads associated with ductile failure modes; brittle failure modes (e.g., shearing out, splitting perpendicular to grain) are not foreseen [5]. Because the EYM does not allow the simulation of brittle failure modes, design codes prescribe empiric minimum dimensions for connections (e.g., dowel holes to end member distances) to avoid the brittle failure modes. In addition to the minimum distances suggested by EC5 [3], the fastener slenderness may be controlled to allow ductile failure modes.

Generally, in order to verify the influence of parameters governing the mechanical behaviour of connections, a number of tests are required for assessing the embedding strength. These embedding tests are standardized such as in the EN383 standard [6].

Alternatively to the EYM, 2D models have been proposed: non-linear beam on elastic foundation models [5, 7] and finite element (FE) models [5, 8-10]. However, these models do not predict the brittle failure modes. The Finite Element Method has been used to simulate the non-linear behaviour of dowel-type wood connections involving different strategies, namely using constitutive models and failure criteria for specific failure modes [8-14], or using Linear Elastic Fracture Mechanics [15-17].

This paper presents experimental and numerical results from monotonic quasi-static compression tests of a double-shear single dowel wood connection, made of *Pinus pinaster* wood, which is one of the species with large implantation in Portugal. Despite the abundance of this raw material, its use for structural applications has been disregarded due to several reasons, such as cultural and lack of data about the behaviour of this material.

The experimental program included tests of single-doweled T-connections. The T-connection consists of three wood members: two simply supported side members loaded along the perpendicular-to-grain direction and a centre member loaded in compression along the parallel-to-grain direction, according to the recommendations of the EN26891 standard [18]. The load–slip behaviour of the joint is determined until failure, including the characterization of the ultimate loads and the ductility.

The connection configuration originated the occurrence of both ductile and brittle failure modes. For this reason, the numerical modelling included a plasticity model, to simulate the ductile behaviour observed essentially in the centre member, and a cohesive damage model implemented along with contact finite elements, to simulate the splitting occurred on side members. A three dimensional FE model of the wood connection is built using the commercial FE analysis code, ANSYS® [19]. The dowel is modelled as isotropic elastic material; wood is considered as orthotropic elastic-plastic material, following the Hill's criterion, in a similar approach applied by Moses and Prion [11-13]. Cohesive elements were added to the side members at locations where brittle failures are likely to occur. The interaction between dowel and wood members is simulated using standard contact finite elements, namely surface-to-surface contact elements available in the ANSYS®. This approach involving mixed plasticity and cohesive damage modelling, is similar to the one followed by Kaliske and Resch [20, 21]. It should be noted that there is already experience documented in the literature about the fracture modelling of pine wood (the same species adopted in this study), using exclusively cohesive damage models [22, 23], but assuming the material in the elastic domain. The non-linear behaviour of the connection is evaluated and compared with the experimental data, allowing the calibration of the proposed models.

EXPERIMENTAL RESULTS AND ANALYSIS

The experimental program consisted of a series (10 tests) of a single-doweled T-connection. Each specimen comprises three wood members: a centre member loaded in compression along the parallel-to-grain direction and two simply supported side members loaded along the perpendicular-to-grain direction (see Fig. 1 and 2). The supports consisted of steel pipes with an inside diameter of 28 mm and an outside diameter of 34 mm. The distance



between the centres of the supports (span) was 426 mm. The load transfer between wood members was assured by means of a steel dowel, which is representative of the most common joining technique in wooden structures. Wood members were cut aligned with the wood grain orientations, as illustrated in Fig. 1. The thickness direction was chosen to correspond to the tangential direction of the wood. All tests were performed with a steel dowel with a nominal diameter, $d = 14$ mm. The nominal thickness of each wood member was 30 mm.

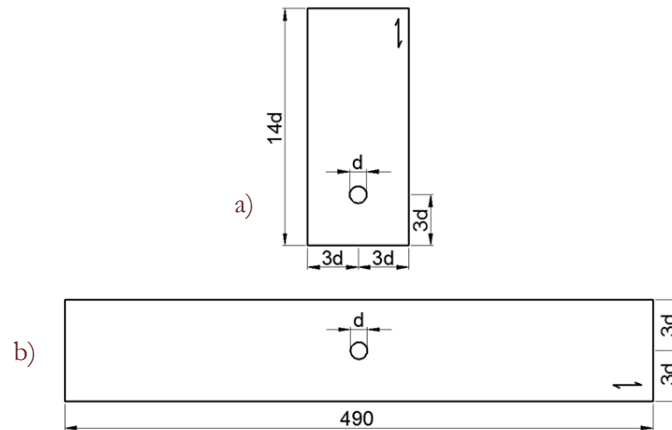


Figure 1: Geometry and dimensions (in mm) of the single-doweled T-joint ($d=14$ mm): (a) centre member; (b) side members.

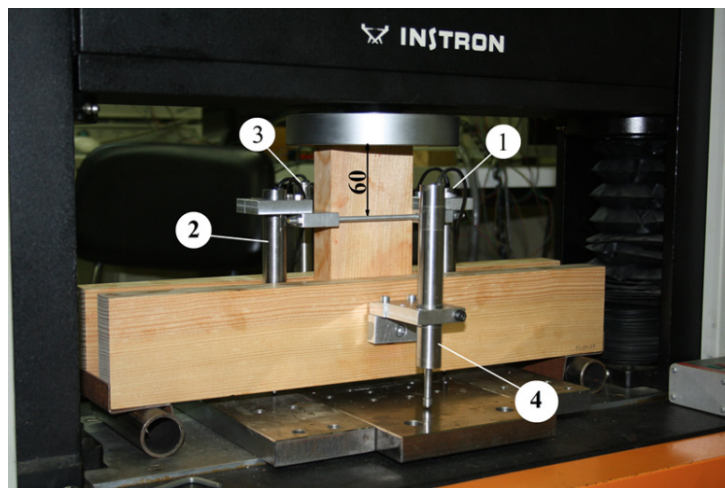


Figure 2: Test apparatus adopted for the T-connections.

Tests were performed on an INSTRON[®] machine, model 1125, rated to 100 kN, under crosshead displacement control. Four linear variable differential transducers (LVDT) were used to measure the displacements (see Fig. 2): two LVDTs (1 and 2) were attached to the centre member to measure the displacement between a section of this member and the machine base; the other two LVDTs (3 and 4) were directly connected to the dowel ends in order to measure the displacement between the dowel and the base of the machine. The LVDTs used in the experimental program were from Applied Measurements[®] with the reference AML/EU ± 10 -S10 (measurement range of ± 10 mm). The data were acquired by means of a SPIDER[®] 8-30 system. A loading–unloading–reloading procedure was adopted, as suggested in the EN26891 standard [18]: firstly, specimens were loaded until 40% of the maximum estimated load (F_{est}), and the crosshead position held for 30s; after this stage, specimens were unloaded until $0.1F_{est}$, and the crosshead position again maintained for 30s; finally, specimens were reloaded until failure. Preliminary tests showed a maximum load of 16500 N. These strength values were the basis for planning the final tests, namely, for the definition of the initial loading cycles according to the procedures provided on the EN26891 standard. The connection was tested with a displacement rate of 0.3 mm/min. Wood densities were measured for each specimen member before testing. The average density was 612.8 ± 30.7 kg/m³. Wood members used in T-joint tests were placed in the laboratory several weeks before testing to allow the wood

to stabilize with the laboratory environment. During the tests, the laboratory temperature was kept between 20 °C and 25 °C.

The specimens used in the single-doweled T-connections were made of maritime pine wood (*Pinus pinaster* Ait.), that were manufactured from trees harvested in the region of Viseu (Portugal). Trees with straight stems (absence of reaction wood) and diameters at breast height of approximately 400 mm were selected. Three-meter-long logs were cut from the sample trees between three and six meters above the basal plane. The logs were live-sawn into thick boards that were kiln-dried to a moisture content between 10% and 12%. The specimens were cut from these boards by aligning the parallel-to-grain direction with the length of the specimens and the wood tangential direction with the thickness of the specimens, as depicted in Fig. 3. Wood with knots, resin pockets, or other type of defects was excluded to reduce the usual scatter observed in timber tests.

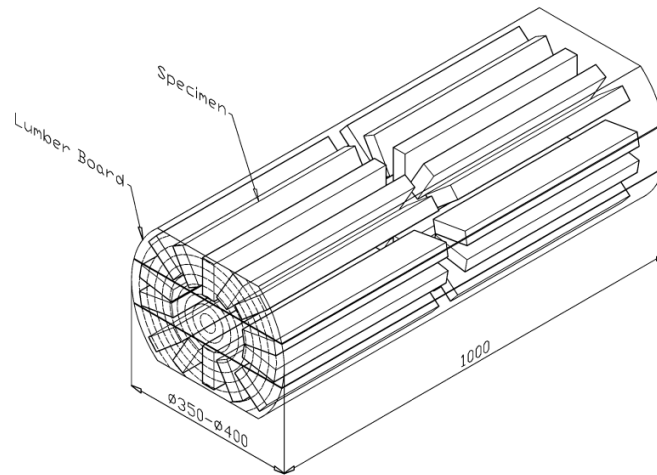


Figure 3: Procedure for the extraction of specimens from a log of a tree (dimensions in mm).

Tab. 1 summarizes the main elastic properties of maritime pine wood, which have been assessed by Xavier *et al.* [24, 25]. These authors performed their work using wood samples from trees harvested in the same region and with similar dimensions of trees used to extract the wood for this research. Therefore, it is expected that the properties proposed by Xavier *et al.* [24, 25] are representative of the wood samples used in this investigation. The elastic moduli (E) are given for the longitudinal (L), radial (R), and tangential (T) directions. In addition, the Poisson ratios (ν) and the shear moduli (G) are presented for the LR, RT, and TL planes. High anisotropic properties are verified for this wood species, which makes connections made of this material more susceptible to cracking due to perpendicular-to-grain tensile stresses.

$E_L = 15.1 \text{ GPa}$	$\nu_{LR} = 0.47$	$G_{LR} = 1283 \text{ MPa}$
$E_R = 1.91 \text{ GPa}$	$\nu_{RT} = 0.59$	$G_{RT} = 264 \text{ MPa}$
$E_T = 1.01 \text{ GPa}$	$\nu_{TL} = 0.05$	$G_{TL} = 1117 \text{ MPa}$

Table 1: Elastic properties of Maritime pine [24, 25].

The load and displacements from four LVDTs were recorded during the experimental tests of the T-connections. Two types of direct displacement measurements were performed, namely, the displacement of a section of the middle wood member, located 60 mm from the loading plate (average displacements of LVDTs 1 and 2), and the displacements of the dowel ends (average displacements of LVDTs 3 and 4), both in relation to the machine base (see Fig. 2). In addition to the previous displacement measurements – (1/2) and (3/4) displacements – the connection slip was computed as the difference between the previous displacements, (1/2)–(3/4). The difference in displacements represents the embedding of the middle member with respect to the dowel. The displacements and connection slip are presented in Fig. 4. The analysis of Fig. 4 shows that the displacements measured at the centre member ((1/2) displacement) are higher than the displacements measured directly on dowel ends ((3/4) displacement). On effect, LVDTs 1 and 2 take into account the total deformation of the centre and lateral wood members; LVDTs 3 and 4 only accounts for the deformation of the lateral members. The analysis of the load-(1/2) displacement results allows the assessment of the global ductility



behaviour of the connection. With respect to this connection, 6 specimens failed at the side members and 4 failed at the centre member. Fig. 5 illustrates the two referenced failure modes, with the final rupture characterized by cracks propagating in the RL system. When the rupture occurs in the centre member of the connection, it corresponds to a higher ductile behaviour because the crack is preceded by some embedding of the centre member in the dowel. The failure due to cracking of the lateral members corresponds to a global brittle behaviour, with the (3/4) displacement not exceeding 2 mm (see Fig. 4b).

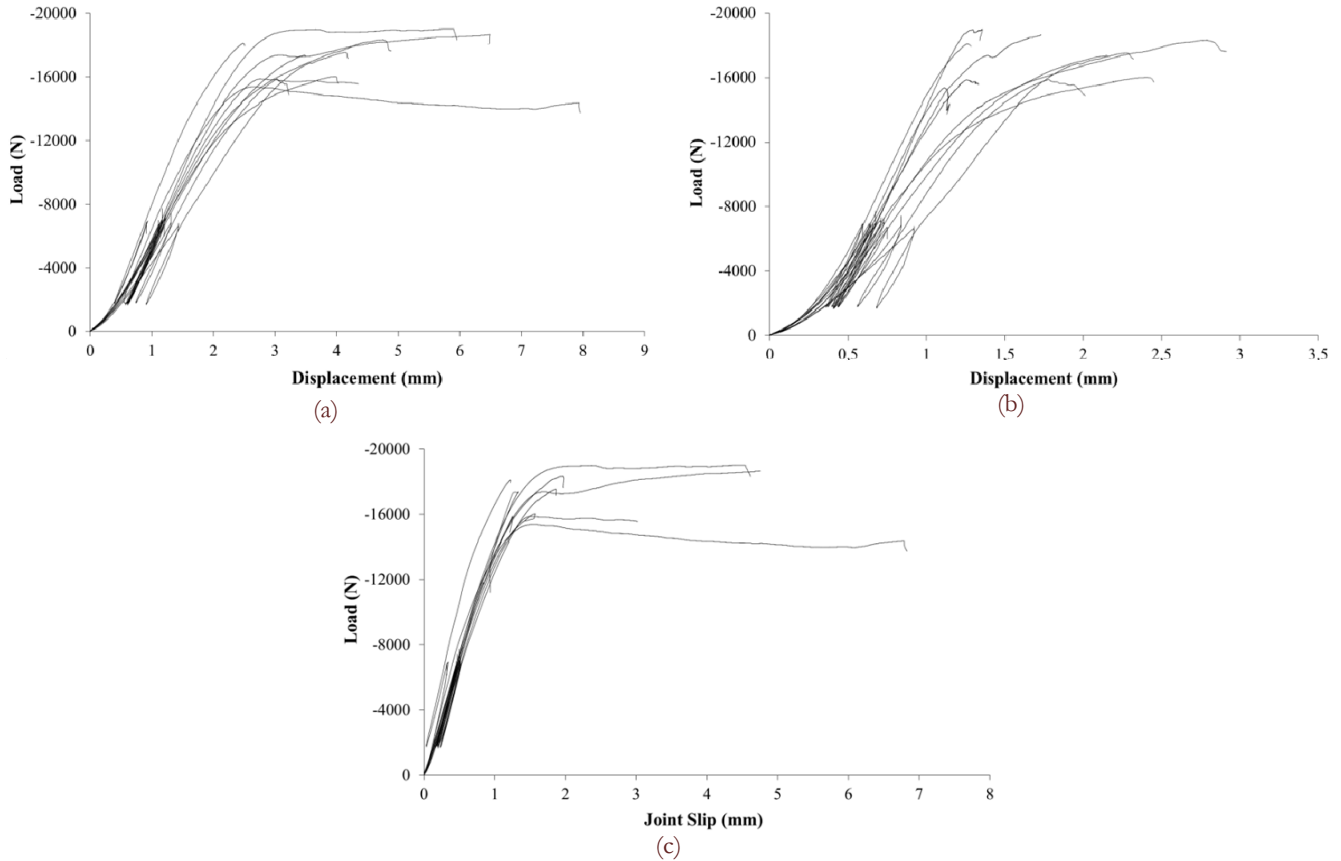


Figure 4: Experimental results: (a) load-(1/2) displacement; (b) load-(3/4) displacement; (c) load-(1/2)-(3/4) joint slip.

Tab. 2 summarizes the average strength and ductility values from the tests: ultimate load, F_{max} ; maximum (1/2) displacement, $D_{(1/2)max}$; maximum (3/4) displacement, $D_{(3/4)max}$; stiffness from (1/2) displacement, k_1 ; stiffness from (3/4) displacement, k_2 and stiffness from (1/2)-(3/4) displacement, k_3 . Experimental average ultimate loads were computed for each one of the two possible failure modes. It is interesting to note that the average ultimate loads are very close to each other, independently of the observed failure modes. However, the majority of the failures were observed on the side members, which may be justified by some size effect. The volume of material involved in the lateral members is twice the volume of the material of the centre member around the dowel; therefore failures are most likely to occur at the side member, for similar stress conditions leading to failure in both members.

Tab. 2 also includes estimates of the failure loads according to the EC5 [3]. According to this design code, the connection strength per shear plane and per fastener is obtained by the expression (1), for the side members:

$$F_{v,R} = f_{h,1} t_1 d \quad (1)$$

and according expression (2), for the case of failure at the centre member:

$$F_{v,R} = 0.5 f_{h,2} t_2 d \quad (2)$$

where $F_{v,R}$ is the load carrying capacity per shear plane and per fastener; $f_{h,i}$ and t_i are, respectively, the embedment strength and the thickness of wood member i ($i=1$ for side members; $i=2$ for centre member) and d is the dowel

diameter. The previous relations consider that failure occurs due to embedding failure at the wood members. The required embedment strengths for previous formulae were obtained in the literature, specifically for the same wood species, using embedding tests with the same thicknesses ($t_1 = t_2 = 30 \text{ mm}$) and dowel diameter $d = 14 \text{ mm}$ ($f_{h,1} = 21.13.6 \text{ MPa}$; $f_{h,2} = 46.44.2 \text{ MPa}$) [26, 27]. Since the investigated connection shows one dowel and two shear planes, the strength values given by Eq. (1) – (2) were multiplied by 2 to result the total failure loads. It is interesting to note that EC5 produced similar strength values to the experimental results. However, a slightly higher strength value is observed when the failure coincides with the embedment of the centre member. According to the EC5, the smallest strength value from all possible failure modes should be considered for the definition of the design failure load of the joint. In this case, the EC5 would suggest the failure mode corresponding to the embedment of the side members, which agrees with the experimental results that showed the majority of failures at the side members. Despite showing apparent success in the prediction of the ultimate loads, the EC5 does not predict accurately the failure modes since it considers the embedding of the wood members as a failure mode when in the reality the situation is distinct, since crack initiation and propagation controls the ultimate loads (see Fig. 5) and the ductility of the joint.

		Experimental	EC5 [3]
F_{\max} (N)	Side members	17213±1041	17724
	Centre member	17228±1868	19488
$D_{(1/2)\max}$ (mm)		4.7±1.7	-
$D_{(3/4)\max}$ (mm)		1.9±0.6	-
κ_1 (N/mm)		7416±1356	-
κ_2 (N/mm)		14445±3303	-
κ_3 (N/mm)		15546±2480	-

Table 2: Average strength and ductility of the T-joint.



Figure 5: Failure modes of the T-connection: (a) failure at the centre member; (b) splitting at the side members.

NUMERICAL MODELLING

A 3D FE model of the tested joint was built and simulation results are presented and discussed in this section. The commercial FE code ANSYS® was used for this purpose [19]. The ANSYS® parametric design language capabilities – APDL language – were used for this purpose. Both wood members and steel dowel were accounted for in the model. They were modelled using hexahedra isoparametric 20-node elements (SOLID95) with full integration. The contact between the dowel and wood members was modelled applying the contact elements available in ANSYS®, using a surface-to-surface option. The contact between the central and side wood members was also simulated. The CONTA174 and TARGE170 elements were used to model, respectively, the contact and target surfaces, forming the so-called contact pairs. Both surfaces of each contact pairs were assumed flexible. Three contact pairs were considered:

- i) between the dowel and the surface of the hole of the side member;
- ii) between the dowel and the surface of the hole of the centre member;
- iii) between the centre and side members (interface).

The Augmented Lagrange contact algorithm was adopted in the analysis. With respect to this contact algorithm, two important numerical contact parameters need to be defined, namely the normal penalty stiffness factor, FKN, and normal penetration tolerance factor, FTOLN [19]. For the proposed simulations, the following contact parameters were adopted: FTOLN=0.1 and FKN={1.0,0.1,0.006}, the latter respectively for wood-wood contact, dowel-central wood member contact and dowel-side wood member contact. These contact parameters were calibrated by authors on previous elastic simulations of embedding tests along the longitudinal and radial directions, performed on similar wood members [27]. Once the joint geometry admits two planes of symmetry, only 1/4 of the joint was modelled (1/2 of the side member and 1/4 of the centre member). The displacements of the nodes located at the planes of symmetry were restrained along the normal direction to these planes. Fig. 6 shows the FE mesh built for the T-connection, where a mesh refinement around of the dowel is observed. The clearance between the dowel and the holes was assumed equal to 0.1mm which is an average value from experimental measurements. The friction coefficient was assumed equal to 0.5, which has been considered a typical value for steel/wood contact.

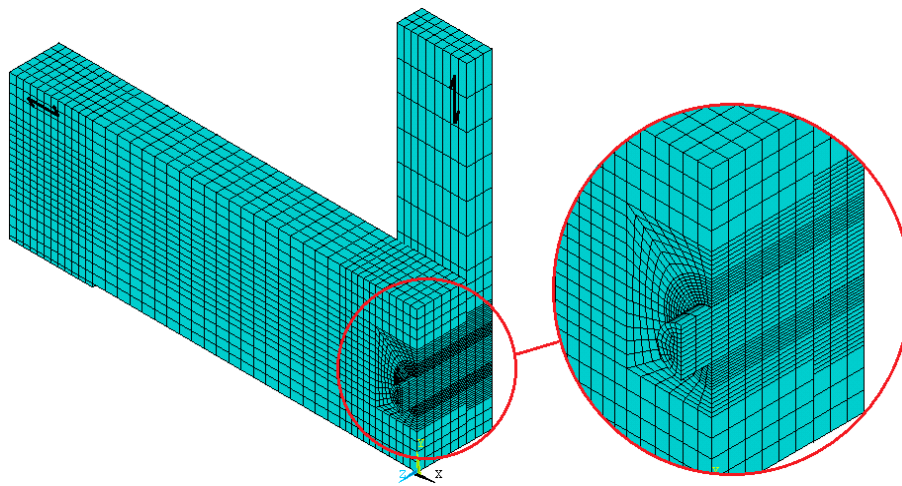


Figure 6: Finite element mesh of the T-connection.

With reference to the constitutive models used in the simulations, the steel dowel was modelled as a homogeneous and elastic material ($E = 210$ GPa; $\nu = 0.3$). With respect to the wood, several constitutive modelling alternative approaches were tested in this investigation.

As a first approach, wood was simulated assuming a fully elastic behaviour with orthotropic elastic properties, as presented in Tab. 1. However this first analysis revealed an unsatisfactory description of the experimental results since the observed experimental non-linear behaviour of the joint is not captured by the simulation.

A literature review about numerical modelling of wood non-linear behaviour [11-13, 28] reveals plasticity constitutive models as a frequently adopted option. The ANSYS® code [19] offers a constitutive plasticity model for anisotropic materials, based on Hill's yield criterion. This model requires the definition of a reference non-linear uniaxial stress-strain curve and anisotropic stress ratios that allow the scaling of this reference curve in order to retrieve the material behaviour for each direction. The model does not distinguish tension from compression behaviours of wood. Therefore, the model calibration requires a compromise between these two distinct wood behaviours, taking into account the dominant stresses applied on wood members. This plasticity model, based on Hill's yield criterion, was adopted to simulate the T-joint load-displacement behaviour. The material was assumed transversely isotropic and the reference curve was assumed perfectly plastic. Therefore, the anisotropic stress ratios required for the model identification corresponded to ratios between anisotropic yield stresses. Two alternative approaches were followed for the plastic analysis:

- i) The same plasticity model parameters were used for both wood members (see Tab. 3). This approach is physically more consistent since the materials of each specimen members are the same.
- ii) Distinct plasticity model parameters were used for each wood member (see Tab. 4). This approach try to use independent plasticity parameters adjusted for each wood member of the joint (central and lateral members) in a tentative to produce better global predictions of the mechanical behaviour of the joint.



		Tension/ Compression		Shear		
		L	R / T	LR	RT	LT
Experimental strength values [MPa]		40–98	4.2–9.4	14–16	2.4–4.5	14–16
Adopted yield stresses [MPa]	Central Member	80	6.1	12.8	3.6	12.8
	Side Member					

Table 3: Experimental strength properties and adopted yield values for Pine wood: same constants set used for both wood members [29].

		Tension/ Compression		Shear		
		L	R / T	LR	RT	LT
Experimental strength values [MPa]		40–98	4.2–9.4	14–16	2.4–4.5	14–16
Adopted yield stresses [MPa]	Central Member	90	5.3	12.8	4.1	14.4
	Side Member	85	5.3	11.2	3.2	11.2

Table 4: Experimental strength properties and adopted yield values for Pine wood: distinct constants used for each wood member [29].

Even though the better description of non-linear response of joint, the elasto-plastic simulations are not able to simulate the initiation and propagation of cracks responsible for sudden load drop observed in the joint testing. Therefore, the plasticity modelling strategy is important to describe the ductile behaviour characterizing the joint, but further enhancements are required to deal with brittle features of the failure modes. Cohesive zone damage models can be used to simulate the brittle cracking occurring in the side members of the T-connection under investigation. In this paper, the use of both plasticity and cohesive zone damage models will be explored including their association.

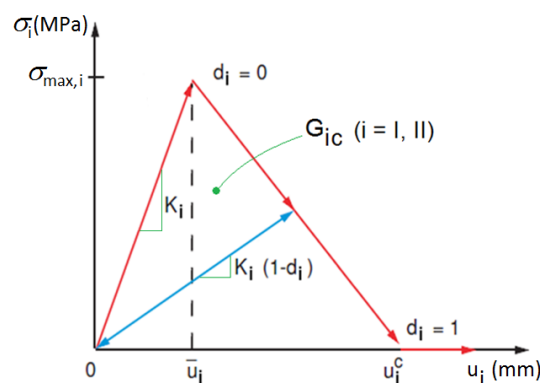


Figure 7: Strength – relative displacement relation for pure modes (adapted from [19]).

The ANSYS® code [19] includes the possibility for cohesive zone damage modelling which can be used to simulate crack propagation at predefined interfaces that can experience decohesion. Consequently, this approach requires the definition of interfaces which can be modelled using interface elements or contact elements. The implementation of the cohesive damage model was performed, in this study, using contact elements. The cohesive damage law adopted was the linear one as defined by Alfano and Crisfield [30]. The damage law for pure fracture modes (I and II) is shown in Fig. 7, where $\sigma_{\max,i}$ represents the onset damage stresses ($\sigma_{\max,I}$: maximum tensile stresses; $\sigma_{\max,II}$: maximum shear stresses). The



mixed mode damage propagation is simulated considering a linear energetic criterion, which takes into account the two fracture modes, according to:

$$\left(\frac{G_I}{G_{IC}}\right) + \left(\frac{G_{II}}{G_{IIC}}\right) = 1 \tag{3}$$

where G_i and G_{iC} are, respectively, the energy release rate and the critical energy release rate ($i = I, II$ stands for fracture pure modes). The fracture properties required for the application of the cohesive damage model were extracted from experimental works performed on Pine wood from the same population, and summarized in Tab. 5 [31]. These fracture properties corresponded to the RL crack propagation system, which is one of the most important crack propagation systems for this wood species ($\sigma_{\max,I} = \sigma_R =$ maximum tensile radial stresses; $\sigma_{\max,II} = \tau_{RL} =$ maximum shear stresses in the RL plane).

σ_R (MPa)	τ_{RL} (MPa)	G_{IC} (N/mm)	G_{IIC} (N/mm)
7.93	16	0.264	0.9

Table 5: Fracture properties for Pine wood: RL propagation system [31].

Tab. 6 presents an overview of simulations performed in this investigation. Besides the fully elastic analysis, two elasto-plastic analyses were performed using the sets of plastic constants given in Tab. 3 (Elastic-plastic (1)) and in Tab. 4 (Elastic-plastic (2)). These tables (Tab. 3 and 4) present suggested yield stresses for tension/compression and shear loadings. Using these yield stresses, the anisotropic ratios were defined taking into account an arbitrary reference curve. Besides the yield stresses adopted for the plasticity model, strength properties extracted from experimental works performed on the same wood species and available in the literature [29], are also presented in the referred tables. These strength properties were used to estimate the yield stresses. The experimental strength properties were presented for both tension and compression longitudinal loading. For radial and tangential directions, only compression strengths were given in the tables (one value for each direction). Concerning the shear strengths, a range of experimental values are given, which resulted from alternative shear testing [29].

Constitutive Modelling Approach	Centre member	Side members
Fully elastic	Orthotropic elastic model with constants from Tab. 1	
Elastic-plastic (1)	Orthotropic elastic model with constants from Tab. 1 Hill's plasticity model with constants from Tab. 3	
Elastic-plastic (2)	Orthotropic elastic model with constants from Tab. 1 Hill's plasticity model with constants from Tab. 4	
Elastic with cohesive	Orthotropic elastic model with constants from Tab. 1	
	-	Cohesive damage model with constants from Tab. 5
Elastic-plastic with cohesive (1)	Orthotropic elastic model with constants from Tab. 1	
	Hill's plasticity model with constants from Tab. 3	Cohesive damage model with constants from Tab. 5
Elastic-plastic with cohesive (2)	Orthotropic elastic model with constants from Tab. 1 Hill's plasticity model with constants from Tab. 3	
	-	Cohesive damage model with constants from Tab. 5

Table 6: Different approaches for the constitutive modelling.

A fully elastic model was also simulated with a cohesive interface on the side member (Elastic with cohesive). The parameters of the cohesive damage model were given in Tab. 5. The model was implemented by means of a contact pair

placed in the side member along the horizontal LT plane containing the hole axis (see Fig. 8). This interface was placed in the most likely position for the initiation and propagation of cracks in the side members.

Besides the simulation of the T-connection using standalone constitutive modelling approaches - plasticity and cohesive damage modelling, two mixed constitutive modelling approaches were also investigated for the joint, as documented in Tab. 6. Firstly, the centre member was considered with elastic-plastic behaviour, through the implementation of the Hill's plasticity model and the lateral member was considered elastic and showing a cohesive interface (Elastic-plastic with cohesive (1)). This approach takes into account the higher embedding strength, experimentally verified in the centre member. Finally, all wood members were assumed elastic-plastic and the cohesive interface on the side member was preserved (Elastic-plastic with cohesive (2)). In both approaches, the Hill's plasticity model was applied, using the constants of the Tab. 3. The cohesive damage model parameters from Tab. 5 were maintained.

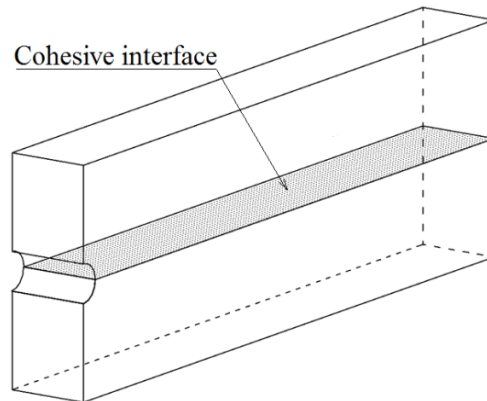


Figure 8: Cohesive interface representation.

Results and discussion

In this section, the results of numerical simulations, using the constitutive modelling approaches summarized in Tab. 6, will be presented and compared with the experimental results, particularly the load-displacement curves obtained for the T-joint. Fig. 9 compares the numerical responses from the simulations with plasticity models. The load-displacement curves shown in Fig. 9 under the “elastic-plastic (1)” series were obtained using the same plasticity constants for both wood members. The consideration of distinct plasticity constants, for each wood member, resulted in an improved load-displacement curve, as demonstrated by the “elastic-plastic (2)” series (see Fig. 9).

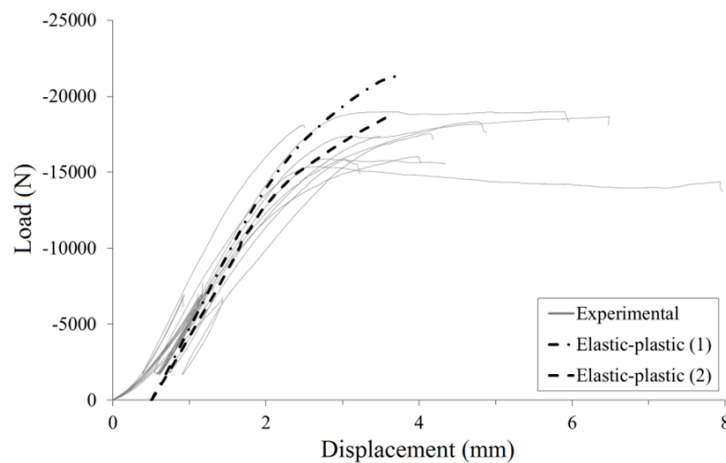


Figure 9: Load-displacement curves: experimental vs. elastic-plastic analysis results.

The experimental curves exhibit a non-linearity at the beginning of tests, which is due to some initial embedding between the steel dowel and wood, motivated from wood surface damage due to the drilling/cutting process, surface imperfections and small misalignments. The numerical models do not describe this behaviour; therefore numerical curves were subjected to a horizontal shift of 0.5 mm. In general, the numeric curves reproduced satisfactorily the initial part of the test results

(elastic stiffness). In addition, the curve obtained with distinct plastic parameters calibrated for each direction (“Elastic-plastic (2)” series), showed better performance at the beginning of the yield region.

The experimental analysis revealed that the T-connection exhibited two distinct failure modes: a dominant ductile failure mode, when it occurs at the centre member and a dominant brittle failure mode when it occurs at the side members. With respect to the stress distributions, it was observed (see Fig. 10) that the maximum shear stresses, in the RL plane, occurred at the centre member and the maximum direct stresses, along the radial direction, occurred in the side members, in both cases at the vicinity of holes. The centre member shows a shear (RL plane) stress concentration above the hole, at locations where cracks were observed to initiated and propagated (see Fig. 5). In the side member, significant radial tensile stresses was verified in the hole surface at the horizontal mid-plane. These tensile stresses can be related to the failure modes occurred in those members (see Fig. 5). Results illustrated in Fig.10 were obtained for the elasto-plastic analysis with similar plastic constants for each wood member. However the previous discussion is also valid if distinct plastic constants were used for each wood member.

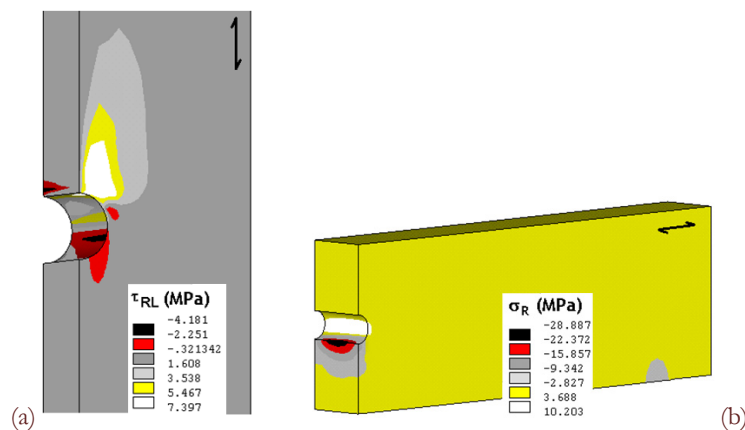


Figure 10: Stress fields from elastic-plastic analysis, using constants from Tab. 3: (a) centre member; (b) side member (F=14kN).

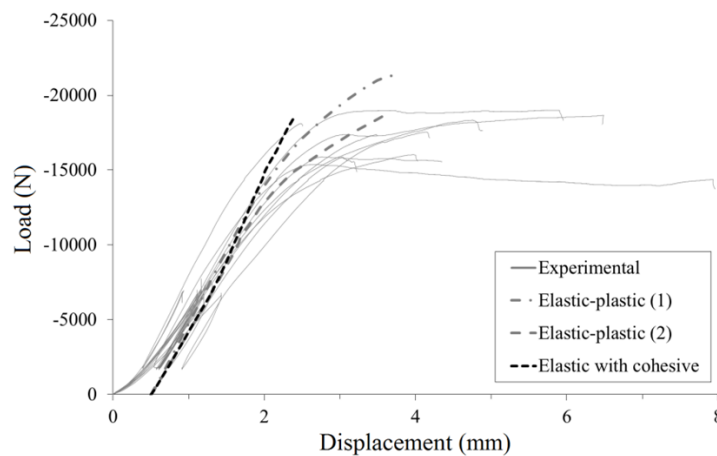


Figure 11: Load-displacement curves: experimental vs. elastic-plastic and elastic with cohesive damage modelling.

Fig. 11 presents the experimental data with the numerical load-displacement curves resulting from the exclusive application of plasticity models and also resulting from the use of a full elastic model with a cohesive damage interface on the side member. The later numerical result exhibits a near linear behaviour until failure and slightly higher elastic stiffness than resulted from the application of the plasticity models. The cohesive damage model with elastic simulation did not provide any load reduction before the crack propagation onset; therefore a typical brittle behaviour is modelled. The cohesive damage model was able to prevent the unbounded load growing. The simulation was performed until a crack initiated and propagated under unstable conditions. Thus, it is demonstrated the good performance of the cohesive model in predicting the ultimate load. In Fig. 12, the nodal relative opening displacements of crack faces are quantified, confirming a corner crack, with a maximum crack opening of about 0.19 mm, at the unstable crack propagation onset. Fig. 13b illustrates the resistance degradation (evolution of radial stresses) in the interface nodes located at the hole surface

of lateral member (see Fig. 13a). Also, it is verified that most of nodes have suffered a total resistance degradation; only the pair of nodes farthest away from the interface between the two wood members, did not reached their total decohesion before unstable crack propagation.

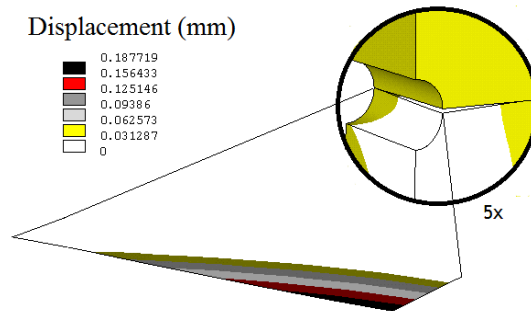


Figure 12: Crack opening displacement – elastic plus cohesive model results.

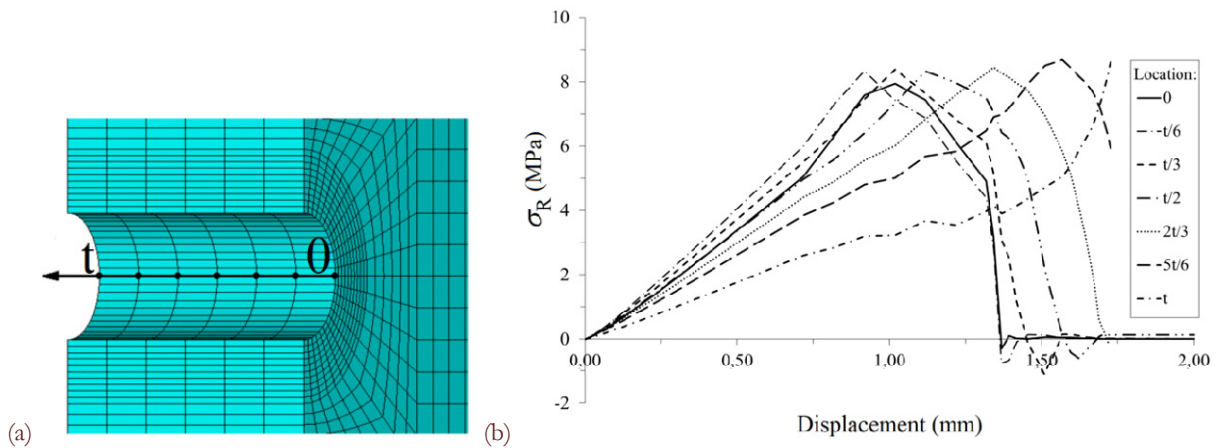


Figure 13: Radial stress evolution at the nodes situated in the interface on the hole surface (elastic plus cohesive damage modelling): (a) nodes location; (b) stress-displacement relation.

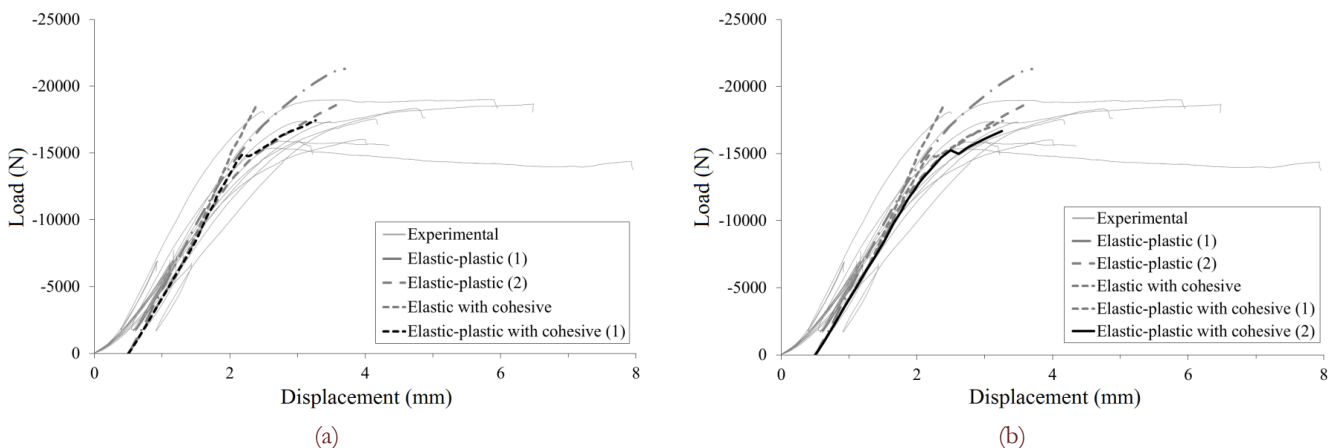


Figure 14: Load-displacement curves: experimental vs. numerical results: (a) side member with elastic behaviour and cohesive damage modelling and centre member with plastic behaviour; (b) members with elastic-plastic behaviour and cohesive damage modelling at side member.

Fig. 14a compares the load-displacement curves from previous simulations and the one resulted from an elastic-plastic behaviour for the centre member and an elastic simulation with cohesive interface for the side member (“elastic-plastic with cohesive (1)” series). In addition, Fig. 14b presents the results obtained simulating all wood members with elasto-plastic behaviour and using a cohesive interface in the side member (“elastic-plastic with cohesive (2)” series). The analysis

of results shown in Fig. 14 reveals a significant improvement in the numerical response, both in terms of ductility and ultimate loads prediction. The simulations assuming elastic-plastic behaviour in all wood members only produced a slight global strength reduction, confirming the little plastic deformation verified in the side members. However, the global response based in this simulation resulted in a better approximation with respect to the experimental data. A local peak was observed in the resulting P-d curves, which is due to the crack initiation. With respect to the crack configuration (see Fig. 15a), the “elastic-plastic with cohesive (1)” approach resulted in a corner crack, similarly to the crack observed with the simulation presented in Fig. 12, but lower opening displacement values were observed (Fig.15b). The “elastic-plastic with cohesive (2)” resulted in an approximately central crack in the side member (see Fig. 16a). In this case, the central nodes were the first ones to reach the rupture strength, starting the process zone at this location (see Fig. 16b). For this case, the complete nodes separation was not verified before unstable crack growth.

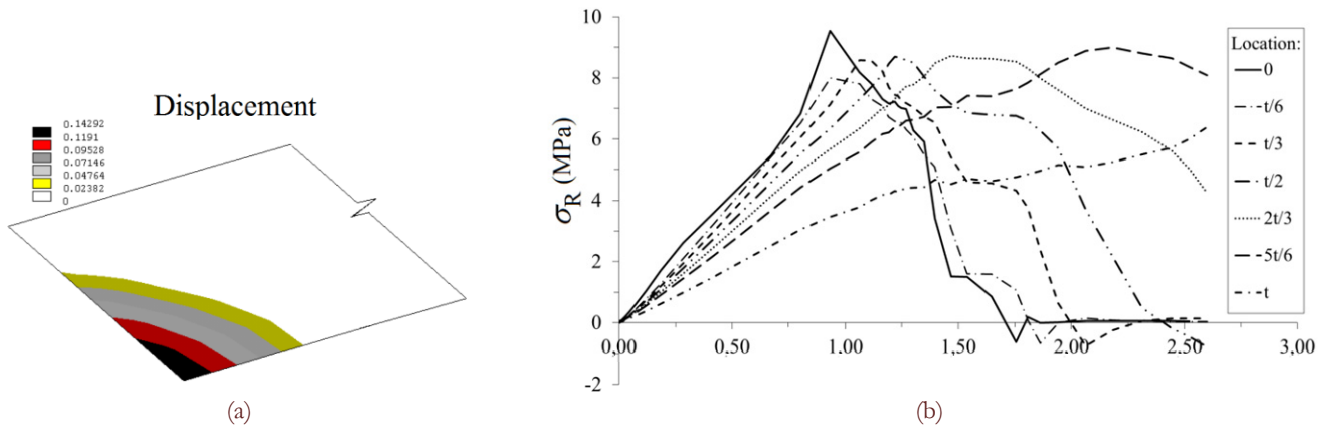


Figure 15: Elastic-plastic model in the centre member + elastic and cohesive damage model in the side member: (a) crack opening displacement; (b) stress-displacement relation at the nodes situated in the interface on the hole surface.

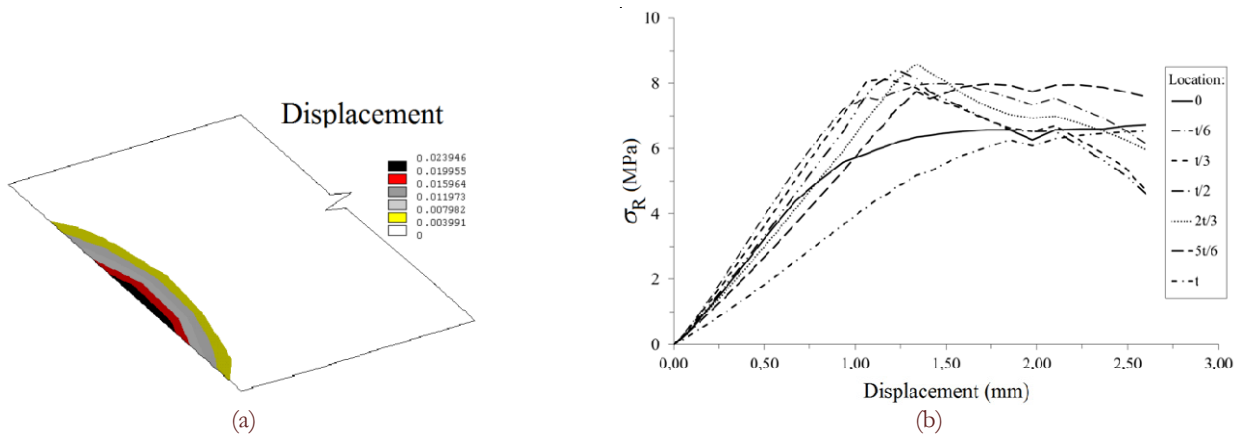


Figure 16: Elastic-plastic model for both members + cohesive damage in the side member: (a) crack opening displacement; (b) stress-displacement relation at the nodes situated in the interface on the hole surface.

CONCLUSIONS

An experimental and numerical characterization of the mechanical behaviour of a type of doweled wood joints was investigated. In this particular case, the investigation was carried out over a T-joint with a central member loaded along the longitudinal or grain direction and the side member loaded perpendicularly to the grain direction. The tested T-joint exhibited both ductile and brittle failure modes. While the failure at side wood members corresponded to brittle failure modes, the failure at the central member corresponded to ductile failure modes. The application of EC5 rules allowed accurate predictions of the ultimate loads even considering that EC5 rules used for this calculation does not



account for brittle failure modes. However the EC5 procedures do not allow the prediction of the complete load-displacement behaviour of the joint.

Numerical simulations were performed considering distinct alternative constitutive modelling strategies. The T-joint simulation assuming elastic-plastic behaviour for both wood members allowed for a non-linear description of joint behaviour, but the ultimate loads related to the collapse of the connection were not accurately described. The use of cohesive damage models enables the simulation of failure modes and respective collapse loads. However, the exclusive use of cohesive damage models with elastic materials provides load-displacement curves without ductility. The simultaneous use of plasticity models with cohesive damage models, allowed the reproduction of both ductility and connection collapse. In the simulated example, the assumption of an elastic behaviour with cohesive damage, for the side member, also revealed satisfactory results, if the central member is simulated as a plastic material. The initial crack in the side member exhibits a shape change, from corner to almost centre crack, when the elastic-plastic behaviour was imposed to this member. This crack configuration needs experimental validation.

REFERENCES

- [1] Itany, R.Y., Faherty, K.F., *Structural wood research, state-of-the-art and research needs*, ASCE, New York, (1984) 210.
- [2] Soltis, L.A., Wilkinson, T.L., *Bolted-connection design*, General technical report FPL-GTR-54, Forest Products Laboratory – USDA, Madison, WI, (1987).
- [3] EN1995-1-1 *Design of timber structures. Part 1-1: General rules and rules for buildings*, CEN, Brussels, (2004).
- [4] Johansen, K.W., *Theory of timber connections*, Int Assn Bridge Struct Eng Pub. 9, Zurich, Switzerland, (1949) 249–311.
- [5] Patton-Mallory, M., Pellicane, P.J., Smith, F.W., *Modelling bolted connections in wood: review*, J Struct Eng, 123 (1997) 1054–62.
- [6] EN383: *Timber structures. Test methods. Determination of embedding strength and foundation values for dowel-type fasteners*, CEN, Brussels, (2007).
- [7] Sawata, K., Yasamura, M., *Estimation of yield and ultimate strengths of bolted timber joints by nonlinear analysis and yield theory*, J Wood Sci, 49 (2003) 83–91.
- [8] Chen, C.J., Lee, T.L., Jeng, D.S., *Finite element modelling for the mechanical behaviour of dowel-type timber joints*, Comput Struct, 81 (2003) 2731–2739.
- [9] Racher, P., Bocquet, J.F., *Non-linear analysis of dowelled timber connections: a new approach for embedding modelling*, Electron J Struct Eng, 5 (2005) 1–9.
- [10] Kharouf, N., McClure, G., Smith, I., *Elasto-plastic modelling of wood bolted connections*, Comput Struct, 81 (2003) 747–54.
- [11] Moses, D.M., Prion, H.G.L., *A Three-Dimensional Model for Bolted Connections in Wood*, Can J Civil Eng, 30 (2003) 555-567.
- [12] Moses, D.M., Prion, H.G.L., *Stress and Failure Analysis of Wood Composites: A New Model*, Compos Part B-Eng, 35 (2004) 251-261.
- [13] Moses, D.M., Prion, H.G.L., *Anisotropic Plasticity and the Notched Wood Shear Block*, Forest Prod J, 52 (2002) 43-54.
- [14] Patton-Mallory, M., Cramer, S.M., Smith, F.W., Pellicane, P.J., *Nonlinear Material Models for Analysis of Bolted Wood Connections*, J Struct Eng, 123 (1997) 1063-1070.
- [15] Yasamura, M., Daudeville, L., *Fracture of Multiply-Bolted Joints Under Lateral Force Perpendicular to Wood Grain*, J Wood Sci, 46 (2000) 187-192.
- [16] Ballerini, M., Rizzi, M., 2007, *Numerical analyses for the prediction of the splitting strength of beams load perpendicular-to-grain by dowel-type connections*, Mater Struct, 40(1) (2007) 139–149.
- [17] Daudeville, L., Yasamura, M., *Failure Analysis of Timber Bolted Joints by Fracture Mechanics*, Mater Struct, 29 (1996) 418-425.
- [18] EN26891-*Timber structures – Joints made with mechanical fasteners – General principles for the determination of strength and deformation characteristics*, (1991).
- [19] Swanson Analysis Systems Inc., ANSYS® Version 12.0, Houston, (2009).
- [20] Resch, E., Kaliske, M., *Three-dimensional numerical analyses of load-bearing behavior and failure of multiple double-shear dowel-type connections in timber engineering*, Comput Struct, 88 (2012), 165-177.



- [21] Resch, E., Kaliske, M., Numerical analysis and design of double-shear dowel-type connections of wood, *Eng Struct*, 41 (2012) 234–241.
- [22] Dourado, N.M.M., de Moura, M.F.S.F., Morais, J.J.L., Silva, A.L., Estimate of Resistance-Curve in Wood Through the Double Cantilever Beam Test, *Holzforschung*, 64 (2010) 119-126.
- [23] Silva, M.A.L., Morais, J.J.L., de Moura, M.F.S.F., Lousada, J.L., Mode II Wood Fracture Characterization Using the ELS Test, *Eng Fract Mech*, 74 (2008) 2133-2147.
- [24] Xavier, J., Garrido, N., Oliveira, M., Morais J.L., Camanho, P.P., Pierron, F., A comparison between the Iosipescu and off-axis shear test methods for the characterization of *Pinus pinaster* Ait, *Compos Part A*, 35 (2004) 827–40.
- [25] Xavier, J., Oliveira, M., Morais, J., Pinto, T., , Measurement of the shear properties of clear wood by the Arcan test, *Holzforschung*, 63 (2009) 217–25.
- [26] Santos, C.L., de Jesus, A.M.P., Morais, J.J.L., Lousada, J.L.P.C., Quasi-static mechanical behaviour of a double shear single dowel wood connection, *Construction and Building Materials*, 23 (2009) 171-182.
- [27] Santos, C.L., de Jesus, A.M.P., Morais, J.J.L., Lousada, J.L.P.C., A comparison between the EN 383 and ASTM D5764 test methods for dowel-bearing strength assessment of wood, *Strain*, 46 (2010) 159-174.
- [28] Dias, A.M.P.G., Van de Kuilen, J.W.G., Cruz, H.M.P., Lopes, S.M.R., Numerical modelling of the load-deformation behavior of doweled softwood and hardwood joints, *Wood Fiber Sci*, 42 (2010) 480-489.
- [29] De Jesus, A.M.P., Pinto, J.M.T., Morais, J.J.L., Analysis of solid wood beams strengthened with CFRP laminates of distinct lengths, *Constr Build Mater*, 35 (2012) 817–828.
- [30] Alfano, G., Crisfield, M.A., Finite element interface models for the delamination analysis of laminated composites: mechanical and computational issues, *Int J Numer Meth Eng*, 50 (2001) 1701-1736.
- [31] Oliveira, J.M.Q., de Moura, M.F.S.F., Morais, J.J.L., 2009, Application of the end loaded split and single-leg bending tests to the mixed-mode fracture characterization of wood, *Holzforschung*, 63 (2009) 597–602.